THE ARCHIVES OF TRANSPORT

VOL. XXII NO 3 2010
10.2478/v10174-010-0019-9

On Estimation of Residual Stresses in Rails Using Shake-Down Based Method

Michał Pazdanowski*

Received August 2010

Abstract

This paper presents a method, which may be used to determine residual stress distribution in bodies subject to cyclic loads. A mixed global/local version of the Meshless Finite Difference Method (MFDM) is used to devise a discrete computational formulation of a shakedown based residual stress calculation mechanical model for elastic-plastic bodies subject to cyclic loadings.
Several 1D and 2D verification/validation tests are presented, including thorough discussion of results and conclusions regarding the details of computational model. The method developed is applied to determine residual stress distribution in a railroad rail subject to simulated contact load.

Keywords: analysis and modelling, computer assistance in the engineering tasks and scientific research, numerical techniques, mechanical properties

1. Introduction

Rail breakage during service may be very hazardous to operational safety. Heavier axial loads, increased volumes of traffic and axial tensile stress at low temperature due to continuously welded rails (CWR) are believed to be the top driving factors behind this phenomenon [34].

Precise estimation of actual (momentary) stresses in rail is necessary to correctly predict breaking failure risk. The actual stresses in rail may be separated into the following components, introduced during various stages of rail life: manufacturing (roller straightening), laying (welding of CWR), service (repeated rolling contacts

* Cracow University of Technology, Faculty of Civil Engineering, 24 Warszawska St., 31-155 Cracow, Poland.

of changing location and magnitude). Plastic deformation occurring in rail material during all these stages results in development of residual stresses, which may attain very high levels [8,34], thus affecting the operational safety. Current paper deals with an application of simplified shake-down and Melan's theorem [20] based method [25,26], to effectively estimate residual stresses due to repetitive loads of which only an envelope (in terms of both load magnitudeand load location) is known a priori. Brief information on numerical and mechanical model is included and accompanied by results of validation tests. Estimates of residual stress distributions in railhead due to simulated service load follow. Conclusions regarding the developed computational approach are presented finally.

2. Meshless Finite Differences

Meshless Finite Difference Method (MFDM) belongs to a wide class of mesh free methods [1,16,18,22,23,32,35] currently under intensive development in several academic centers. The original method dealt with regular nodal grids [5,7,30], thus severely limiting its applications to regular domains.

Finite Difference Method formulation applicable to irregular grids has been developed beginning in the seventies of the previous century [6,10,13-17,19,21,29,33]. In current work a version of the Meshless Finite Difference Method generalized for arbitrarily irregular grids, proposed in [14-17] and further developed in [11,12,24] is used.

The main idea of the method is to replace the differential operators by the appropriate finite difference operators built on a certain set of nodes, constituting the so called "star". Moreover, when the global method is applied, numerical integration and assembly are performed, as in the FEM.

The idea of the meshless FDM, implemented for two dimensional domains, is briefly described below. In such a case, generation of a finite difference operator is done as follows. An irregular grid of nodes is assumed to be given in an domain Ω. A certain number of neighboring nodes is associated with every node according to a specific criterion (for example a cross criterion, or Voronoi neighbors criterion [16] may be used). Those nodes constitute the so called nodal "star", centered on a node, further called the "central" one (see Fig. 1). At the "central" node the unknown function f is expanded into Taylor series with respect to every node of the star:

$$f_j = f_0 + h_j \cdot \frac{\partial f_0}{\partial x} + k_j \cdot \frac{\partial f_0}{\partial y} + \frac{h_j^2}{2} \cdot \frac{\partial^2 f_0}{\partial x^2} + h_j \cdot k_j \cdot \frac{\partial^2 f_0}{\partial x \partial y} + \frac{k_j^2}{2} \cdot \frac{\partial^2 f_0}{\partial y^2} + O(r^3) = \tilde{f}_j + O(r^3), \quad (1)$$

where:

$$h_j = x_j - x_0, \quad k_j = y_j - y_0, \quad (2)$$

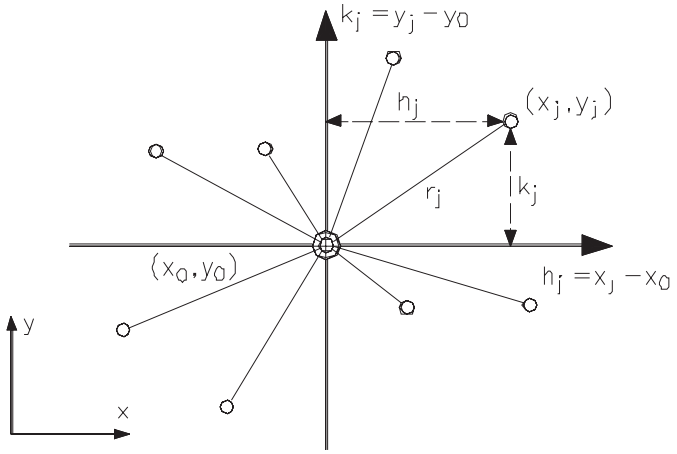

Fig. 1. Irregular "star" for finite difference operator

$$r_j = \sqrt{h_j^2 + k_j^2}. \tag{3}$$

f_i – value of the function $f = f(x, y)$ at a nodal point j belonging to the "star",
f_0 – value of the function at the "central" node, i.e. $f_0 = f(x_0, y_0)$.

A weighted minimization method [14] is now applied to obtain a local approximation of the unknown function $f(x, y)$ by a surface of the requested order $f \cong \tilde{f}$. Thus the following weighted error functional is built in case of the second order surface:

$$B = \sum_{j=1}^{n} \left[\left(-f_j + f_0 + h_j \cdot \frac{\partial f_0}{\partial x} + k_j \cdot \frac{\partial f_0}{\partial y} + \frac{h_j^2}{2} \cdot \frac{\partial^2 f_0}{\partial x^2} + h_j \cdot k_j \cdot \frac{\partial^2 f_0}{\partial x \partial y} + \frac{k_j^2}{2} \cdot \frac{\partial^2 f_0}{\partial y^2} + \ldots \right) \cdot \frac{1}{r^{p+1}} \right]^2 \tag{4}$$

where index j enumerates all nodes belonging to the "star" except the central one and p denotes order of the approximating surface, and at the same time the Taylor series expansion cut-off level. B is minimized with respect to the derivatives of the function f at the point (x_0, y_0):

$$\frac{\partial B}{\partial \{Df\}} = 0. \tag{5}$$

In this manner a set of linear algebraic equations is obtained, which is later solved for the unknown finite difference coefficients at the point (x_0, y_0):

$$\mathbf{A} \cdot \{Df\} = \mathbf{C} \cdot \{f\}, \tag{6}$$

where:

$$\{Df\} = \left\{ \frac{\partial f_0}{\partial x}, \frac{\partial f_0}{\partial y}, \frac{\partial^2 f_0}{\partial x^2}, \frac{\partial^2 f_0}{\partial x \partial y}, \frac{\partial^2 f_0}{\partial y^2} \right\}, \tag{7}$$

$$\{f\} = \{f_1 - f_0, f_2 - f_0, f_3 - f_0, ..., f_n - f_0,\}, \tag{8}$$

and **A** and **C** are matrices dependent only on the star geometry. The set of equations (6) yields the required differential formulas for all the first and second order derivatives

$$^{q}f = {}^{q}\mathbf{B}_{j(i)} \cdot f_j, \tag{9}$$

where:

$$^{q}f = \left\{f_{,x}, f_{,y}, f_{,xx}, f_{,xy}, f_{,yy}\right\}, \tag{10}$$

$^{q}\mathbf{B}_{j(i)}$ – matrix of differential operator coefficients at the node i,
f_j – vector made of the function f values at nodes belonging to the "star" at node i.

The weighted minimization method outlined above may be used to compute approximate value of function as well as to derive the coefficients of finite difference operators. The function f, as well as its derivatives, can be approximated at an arbitrary point (x_0, y_0) like the Gauss station or the equilibrium equations and yield condition application point on the figure below, if the error functional (5) is minimized with respect to f_0 as well as $\{Df\}$. One may take advantage of this fact in the global MFDM in order to approximate values of any integrand to Gaussian station when performing numerical integration (see Fig. 2). Having found the $\{Df\}$ vector, one may also generate any difference operator required in the local MFDM version and obtain the required finite difference equations.

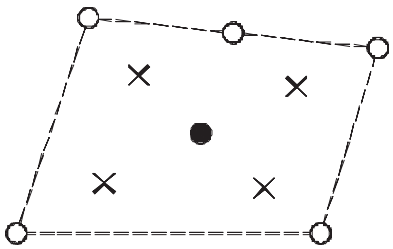

Fig. 2. Approximation and integration between nodes (the dashed line denotes integration subdomain only): ○ – nodes i, × – Gauss stations, ● – equilibrium equations and yield condition application point

3. The Mechanical Formulation

The mechanical problem at hand may be stated as follows [25]: *an estimate of actual residual stresses, induced in a body made of the elastic perfectly plastic material and subject to cyclic loadings may be found using the following constrained optimization approach*:

find:

$$\min_{\sigma^r_{ij}} \Theta\left(\sigma^r_{ij}\right), \Theta = \int_V \left(\sigma^r_{ij} - \sigma^{r_0}_{ij}\right)^T \cdot C_{ijkl} \cdot \left(\sigma^r_{ij} - \sigma^{r_0}_{ij}\right) dV \tag{11}$$

at:

$$\sigma^r_{ij,j} = 0 \quad \text{in } V, \tag{12}$$

$$\sigma^r_{ij} \cdot n_j = 0 \quad \text{on } \partial V, \tag{13}$$

$$\Phi\left(\sigma^r_{ij} + \sigma^e_{ij}\right) \leq \sigma_y \quad \text{in } V, \tag{14}$$

where:

σ_y – yield limit,

σ^e_{ij} – momentary (i.e. time dependent) elastic stresses (determined, as if the considered body behaved in a purely elastic way during the whole loading process history),

σ^r_{ij} – residual stresses induced in the considered body by a given loading program,

$\sigma^{r_0}_{ij}$ – initial residual stresses which existed in the body prior to the current loading program,

C_{ijkl} – elastic compliance matrix.

The minimized formula (11) represents the total complementary energy of the considered body, while formulas (12) – (14) denote the internal equilibrium conditions, homogeneous boundary conditions on the body surface and yield condition, respectively.

The integral formula (11) is of course applied at the whole analyzed body (i.e. globally), while formulas (12) – (14) are applied one point at a time (i.e. locally).

4. Tests and Validation of the Model

Numerous tests have been performed, to fine-tune the parameters of numerical model, such as: numerical integration (around or between nodes, number of points in formula), location of points, at which the linear equality constraints (equilibrium equations and boundary conditions) are applied (nodes or points between nodes), location of points, at which the nonlinear constraints (yield conditions) are applied (nodes or points between nodes), approximation of the stress state between nodes (number of nodes and order of the weighting function used to derive the difference formulas), as well as to verify and validate the mechanical model.

An effort to estimate the influence of: the mesh irregularities on the quality of computed stresses and the rate of convergence to the analytical solution, the plastic zone size, complex stress state and location of the elasto-plastic boundary with respect to the nodes on the quality of estimated residual stress state have been undertaken as well.

4.1. Test problems solved in 1D

A thick walled cylinder, made of elastic-perfectly plastic material, subject to various simple or combined loadings exhibiting radial symmetry and constant along the length of the cylinder has been chosen as a test problem. Readily available analytical solutions of such problem exist for the special case of incompressible material [31,36]. Invariance of loadings along the length of the cylinder led to the analysis in one, arbitrarily chosen cross-section, while the radial symmetry made possible the reduction to only one spatial dimension, along the radius.

Cylinder geometry, material constants and level of loading applied warrant, that the analyzed structure shakes down during the first loading cycle. Three separate loading cases have been considered (see Fig. 3), namely: pulsating internal pressure p (an autofrettage problem), pulsating pure torsion with extreme value of torsional moment equal to M, pulsating torsion M and tension N, acting under a simple (proportional) loading program.

The loading levels have been assumed to ensure plastic deformation of 25%, 50%, 75% and 100% of cylinder thickness.

Three distinct nodal meshes have been applied along the radial direction in order to analyze the phenomena of interest (see Fig. 4). Please note, that in case of torsion and torsion and tension, where plastic zone is located on the outside of the cylinder the actual mesh used is a mirror image of meshes presented in Fig. 4b) through 4d).

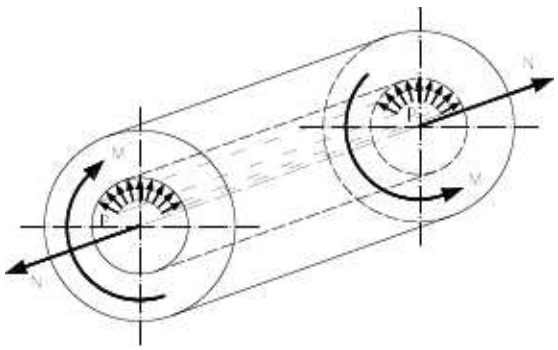

Fig. 3. Thick walled cylinder subject to cyclic loads

4.2. Test results in 1D

Due to the practical considerations (limited space available) only the most interesting from the practical point of view residual stress component (σ_{zz}) is presented (Figs 5, 6), with the exception of the pure torsion test. Here the only non zero residual stress (τ_{rz}) is drawn (Fig. 7).

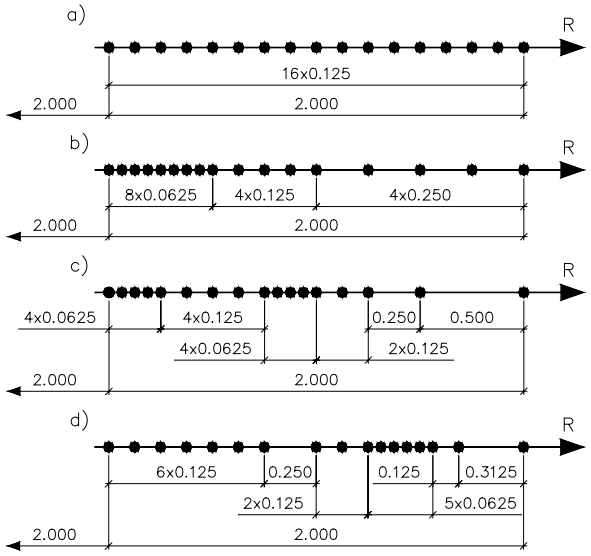

Fig. 4. Nodal meshes used during 1D residual stress analysis: a) regular mesh, b) irregular mesh, 25% of cylinder thickness in plastic zone, c) irregular mesh, 50% of cylinder thickness in plastic zone, d) irregular mesh, 75% of cylinder thickness in plastic zone

All the performed 1D calculations have led to the following conclusions: relatively low order numerical integration is sufficient to obtain results of good quality, while open ended formulas (Gauss type) applied between nodes yield much better results than integration around nodes; equality (equilibrium equations, boundary conditions) and inequality (yield conditions) constraints should be applied between the nodes, this is especially true, when irregular mesh is used; the lower the residual stress approximation order between the nodes, the better the computed residual stress distributions, the weighted minimization derived differential formulas at the lowest possible power of weighting factor yield consistently better results than the standard differential formulas; the irregular mesh of nodes, with properly distributed node concentration zones (the elasto-plastic boundary seems to be especially important) seems to have a significant beneficiary effect on the determined residual stresses in terms of convergence of the calculated results to the known solution, at least with respect to the total complementary energy (see Fig. 8); the plastic zone size, complex stress state and location of the elasto-plastic boundary seem to have no adverse effect on the quality of determined residual stress distributions, when the nodal mesh is dense enough and the nodes are properly distributed.

During the tests it also has been found out, that the proper treatment of the elastic solution yields an additional chance to estimate the quality of determined residual stresses in terms of convergence and convergence limits. Namely, if the nonlinear constraints (yield conditions) are applied between nodes, one may determine elastic solution in such points by two approaches: determine these stresses directly at the

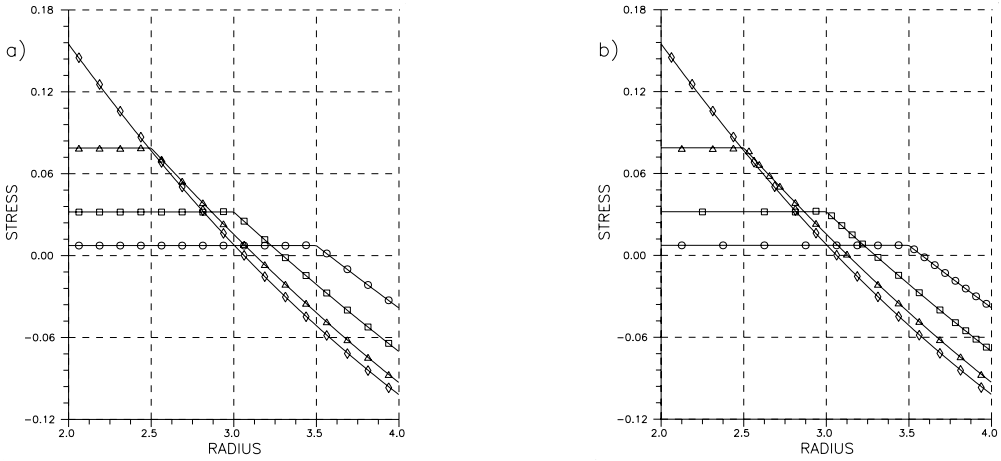

Fig. 5. Residual stress σ_{zz} (along the longitudinal axis) in a thick-walled cylinder (1D case) under pulsating axial force and torsional moment: a) regular mesh, b) irregular mesh. Plastic region depth (as a percentage of cylinder thickness): ◯ – 25% □ – 50% △ – 75% ◇ – 100%. Stress relative to the material yield limit; continuous line - analytical solution

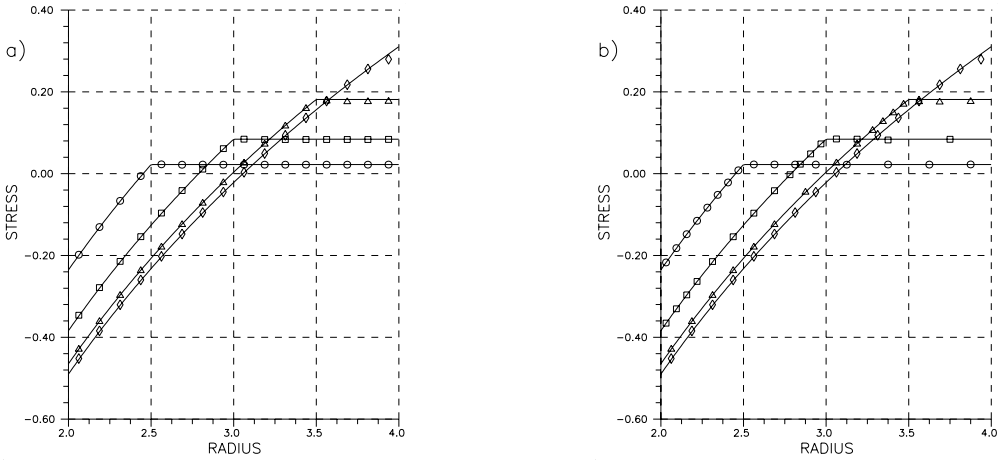

Fig. 6. Residual stress σ_{zz} (along the longitudinal axis) in a thick-walled cylinder (1D case) under pulsating internal pressure (an autofrettage problem): a) regular mesh, b) irregular mesh. Plastic region depth (as a percentage of cylinder thickness): ◯ – 25% □ – 50% △ – 75% ◇ – 100%. Stress relative to the material yield limit; continuous line – analytical solution

necessary points; determine the stresses at nodes and approximate to the necessary points using the same formulas, as used for residual stresses.

The first approach results in convergence to the exact solution from above and the second from below (see Fig. 9).

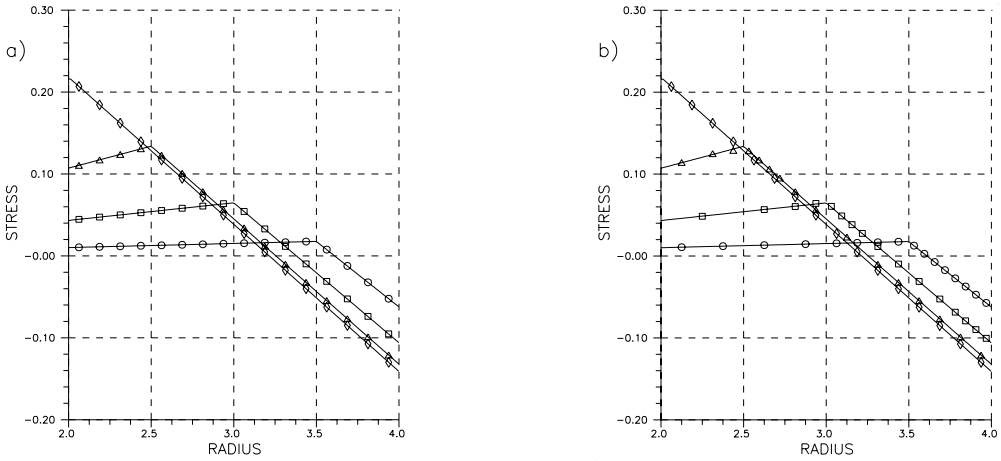

Fig. 7. Residual stress τ_{rz} (along the longitudinal axis) in a thick-walled cylinder (1D case) under pulsating axial force and torsional moment: a) regular mesh, b) irregular mesh. Plastic region depth (as a percentage of cylinder thickness): ◯ – 25% □ – 50% △ – 75% ◇ – 100%. Stress relative to the material yield limit; continuous line – analytical solution

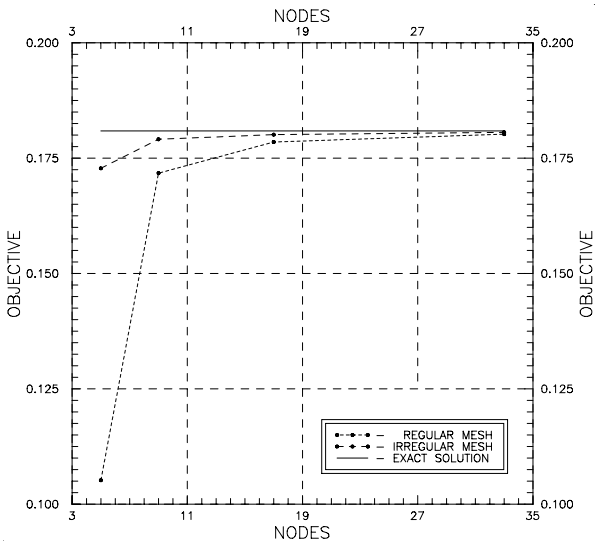

Fig. 8. Convergence of the total complementary energy to analytical solution

4.3. Test problems solved in 2D

The autofrettage problem, with a pulsating load corresponding to the plastic zone reaching 25% of the cylinder thickness has been solved as a 2D problem, in order to: verify the computer code developed to analyze the engineering problems

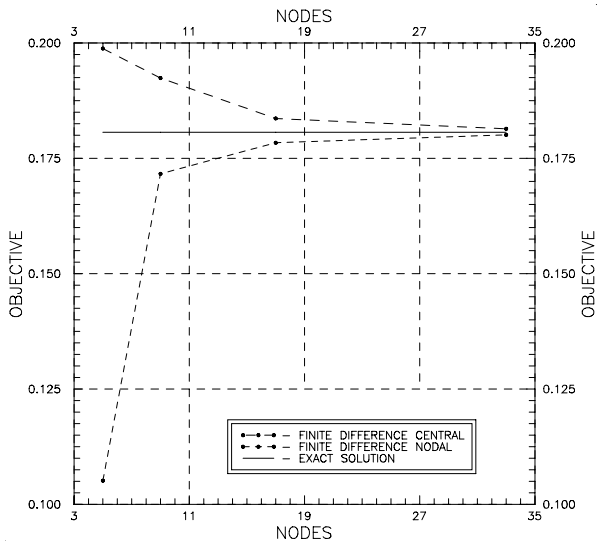

Fig. 9. Convergence of the total complementary energy from above and from below

(railroad rail/vehicle wheel) in 2D; check the conclusions arrived at during 1D analysis.

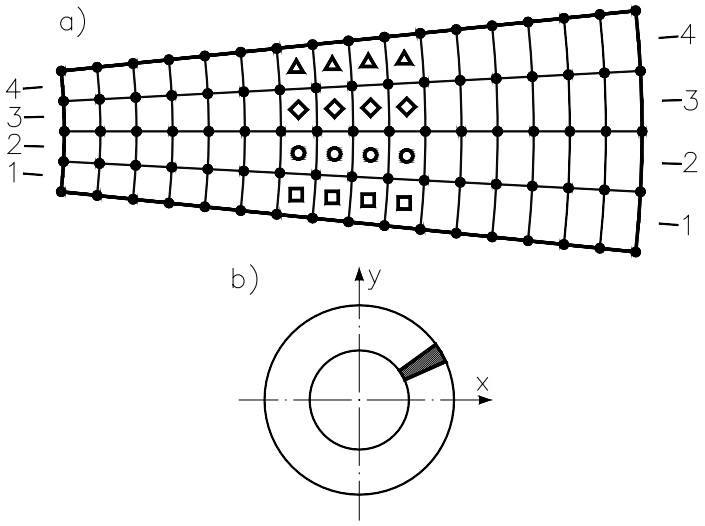

Fig. 10. 2D test problem solved: a) discretization of the cylinder section, b) location of the cylinder section in the global Cartesian coordinate system

The set of quadrilateral integration elements has been spanned over an assumed regular net of nodes (see Fig. 10a)). The equality (internal equilibrium equations) and inequality (yield conditions) constraints have been applied in the centroids of

the quadrilaterals, while the 2×2 Gauss integration rule has been used inside the quadrilaterals. The differential formulas have been generated using the weighted error minimization method with Taylor series expansion truncated after the first order terms. The necessary differential formulas have been generated using four node stars (nodes in quadrilateral vertices).

Calculations have been performed for a 2D section of the cylinder located in the global coordinate system as presented in the Fig. 10b) (the section having angular width of 12° is located so, that it's axis of symmetry is at the 30° angle to the global x axis). All actual calculations have been performed in the Cartesian coordinate system, and afterwards transformed to the cylindrical system of coordinates for presentation purposes.

4.4. Test results in 2D

All the non zero residual stress components, after the transformation to the cylindrical coordinate system are presented above (Fig. 11). The perfect coincidence of computed stresses with the analytical solution indicate that the computational model is valid, computer code is correct, and most of the customizable parameters of the computer model (such as integration type, generation of differential formulas) have been set properly.

During analysis of 1D and 2D tests it has been found out, that centroidal results of residual stresses are much better than the nodal values (in terms of convergence to the known analytical solutions and smoothness), so all the subsequent plots will use the centroidal residual stress values.

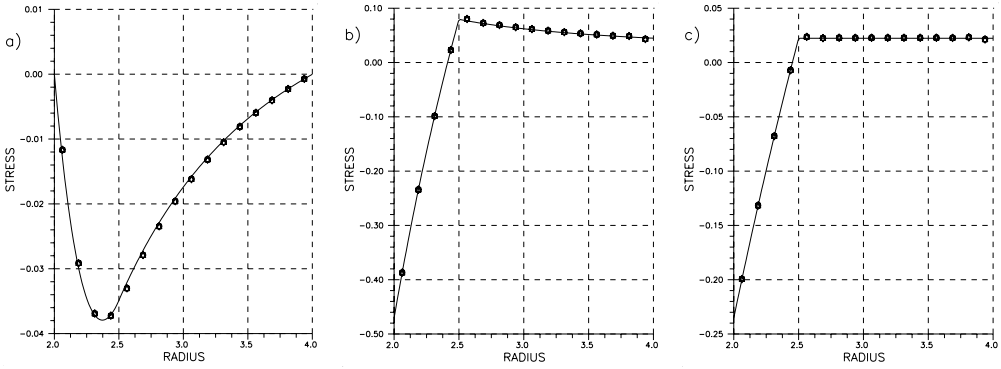

Fig. 11. Thick-walled cylinder subject to pulsating internal pressure: a) σ_{rr}, b) $\sigma_{\theta\theta}$, c) σ_{zz}. Section along the line (Fig. 10a)): ◯ – 1 – 1 , □ – 2 – 2 , ♢ – 3 – 3 , △ – 4 – 4 Analytical solution —

5. Analysis of Residual Stresses in Rail

A true 3D analysis of the residual stress distribution in a railroad rail under simulated service loading has been performed for a 132RE rail (US type) subject to the loading simulated by the contact (Hertzian) pressure applied to the top surface of rail; the pressure had been applied to an area 1,25 cm wide by 2,00 cm deep with a peak value of 1280 MPa (corresponding to the wheel load of 15 t), the material yield limit had been assumed to be equal to 482 MPa. The Young modulus had a value of 207×10^3 MPa and Poisson's ratio 0,3. The track foundation modulus had been equal to 20,7 MPa.

Taking into account the results of previously performed comparative calculations, all the results presented below have been obtained under the following assumptions: quadrilateral differential elements are applied (word element denotes the integration domain only); 3×3 Gauss integration rule is used inside each quadrilateral; internal equilibrium conditions are imposed in the quadrilaterals' centroids; homogeneous boundary conditions are imposed in the midpoints between subsequent boundary nodes; for the quadrilaterals assigned to the computational plastic zone yield conditions are applied in the quadrilaterals' centroids; the weighted error minimization method with Taylor series expansion truncated after the first order terms is used to generate the required differential formulas.

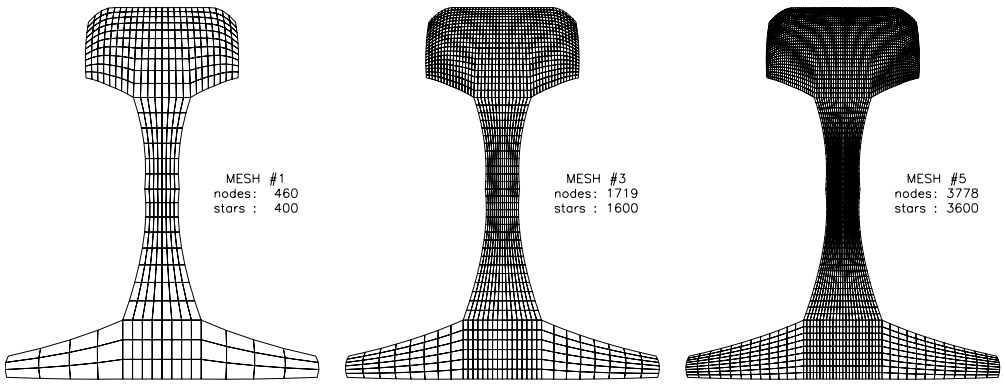

Fig. 12. Meshes used for rail calculations

Numerous computational tests have been performed so far, on five meshes differing in density. Three of the meshes used are presented in the Fig. 12. Results of comparative calculations of the residual stress distributions for a load applied on the rail longitudinal axis of symmetry, performed in order to investigate the mesh density influence on the solution quality (especially in the area of high solution gradients in the immediate vicinity of contact patch) and convergence of the calculated stress distributions are shown in Fig. 13-15, as well as in Table 1. Since the same mechanical model has been incorporated into two other computational models, using

the Boundary Element Method (BEM) [2-4] and Hybrid Finite Element Method (HFEM) [9,27], this opportunity has been used as well to compare the residual stress distributions determined using MFDM and HFEM (see Fig. 14).

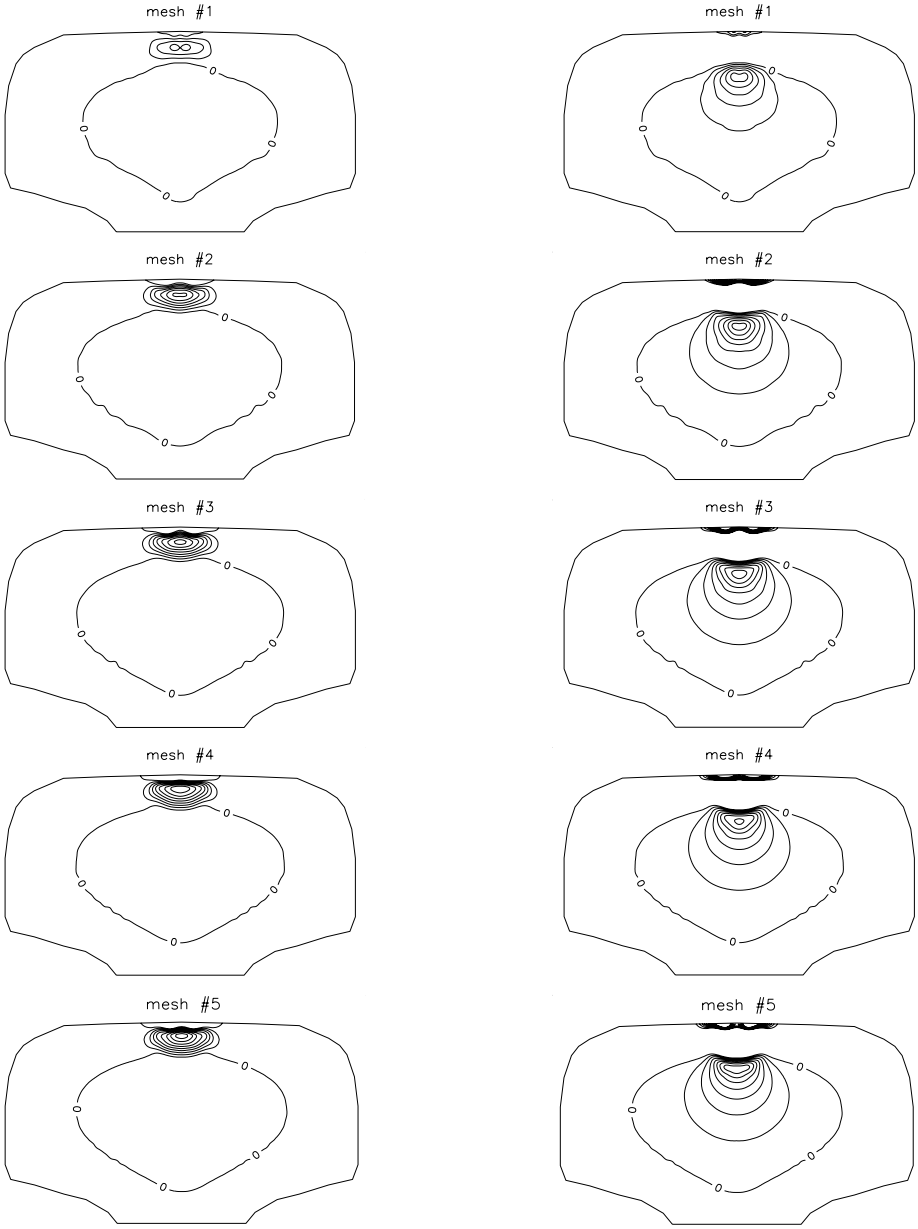

Fig. 13. Convergence test. Contour plots of the σ_{zz} residual stress – meshes 1 through 5: left column – compression (contour interval 21 MPa), right column – tension (contour interval 7 MPa)

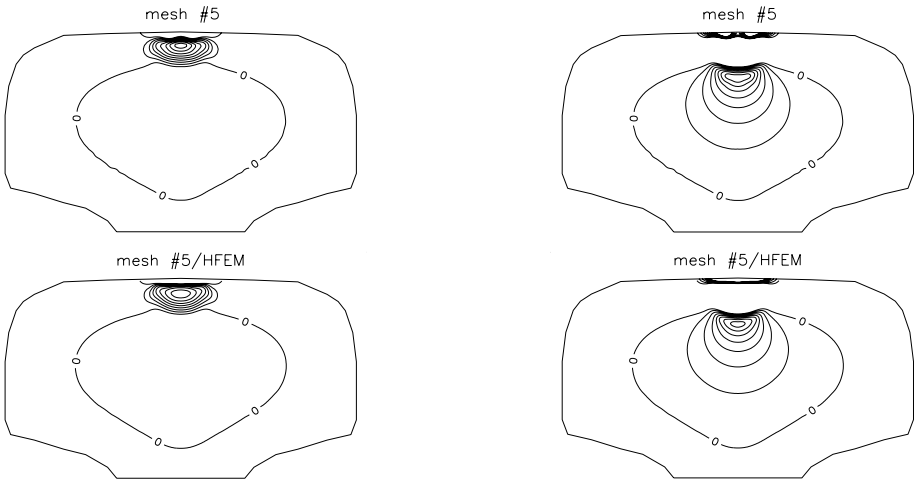

Fig. 14. Comparison MFDM vs. HFEM. Contour plots of residual stress – mesh 5: left column – compression (contour interval 21 MPa), right column – tension (contour interval 7 MPa)

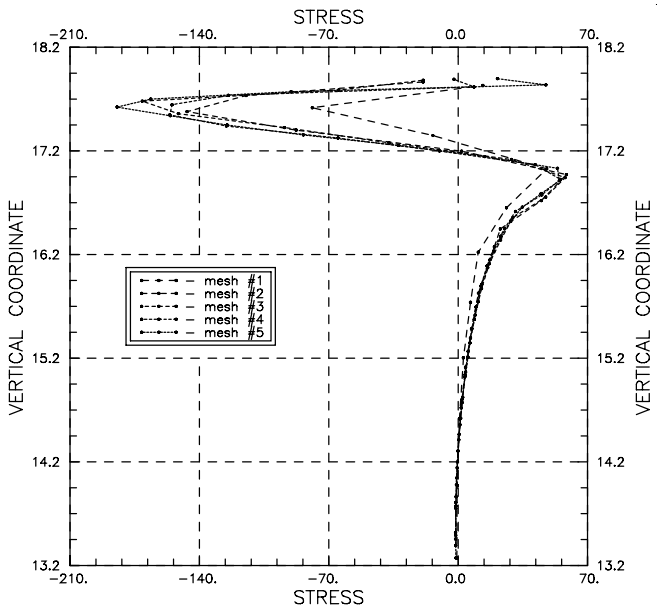

Fig. 15. Residual stress σ_{zz} (in MPa) in railhead on the center-line versus distance from the rail foot (in cm)

Due to the limited space available, only the σ_{zz} residual stress tensor component in the railhead is presented in all figures pertinent to the considered case, due to it's practical importance (it is believed, that this component constitutes the driving

factor of the crack initiation and growth rate). To improve the readability, the contour plots have been split into negative (tensile) and positive (compressive) components. All stress values are in MPa.

The convergence test has been run twice, i.e. for elastic solution determined at nodes and later on approximated to quadrilateral centroids ("nodal" solution), and determined directly at quadrilateral centroids ("central" solution), in order to obtain an lower and upper estimate of the solution, at least in terms of total complementary energy (see Fig. 9). The same test has been performed using the HFEM numerical model [27], and the centroidal values of elastic solution. Results are presented in Fig. 13 through 15.

Table 1

Extreme values of residual stresses, central loading. Convergence test (comparison MFDM-HFEM)

METHOD	**mesh**	**STRESS** [kpsi]							
		σ_{xx}		σ_{yy}		σ_{zz}		σ_{xy}	
		min.	**max.**	**min.**	**max.**	**min.**	**max.**	**min.**	**max.**
MFDM	**1**	-103,83	71,44	-29,77	59,74	-70,77	36,82	-32,85	32,85
	2	-169,48	110,80	-44,49	64,30	-129.61	50,52	-54,22	54,22
	3	-200,18	121,25	-53,92	61,79	-155,33	52,66	-59,57	59,57
	4	-217,64	120,00	-65,76	56,30	-157,07	49,97	-60,36	60,36
	5	-218,62	131,56	-69,98	55,55	-165,15	53,35	-63,89	63,89
HFEM	**1**	-151,28	80,62	-58,73	69,40	-96,91	29,89	-28,69	28,69
	2	-187,14	107,83	-88,87	49,29	134,96	40,96	-40,39	40,39
	3	-193,54	124,93	-90,14	46,02	-149,97	48,44	-51,21	51,21
	4	-204,57	127,55	-84,53	49,15	-157,25	50,21	-56,28	56,28
	5	-221,08	128,12	-86,84	49,71	-156,91	50,66	-59,32	59,32

Table 2

Residual stress tensor extreme values in railroad rail, mesh #5, central loading (comparison MFDM-HFEM)

METHOD	**STRESS** [kpsi]							
	σ_{xx}		σ_{yy}		σ_{zz}		σ_{xy}	
	min.	**max.**	**min.**	**max.**	**min.**	**max.**	**min.**	**max.**
MFDM	-218,62	131,56	-69,98	55,55	-165,15	53,35	-9.268	63,89
HFEM	-221,08	128,12	-86,84	49,71	-156,93	50,67	-8.605	59,33
AVERAGE[1)]	-219,85	129,84	-78,41	52,63	-161,04	52,01	-8.937	61,61
ERROR[2)]	-1,23	-1,72	-8,43	-2,92	4,11	-1,34	0.332	-2,28
ERROR [%][3)]	-0,56	1,32	-10,75	5,54	2,55	2,58	3,71	3,71

[1)] - an arithmetical average of MFDM and HFEM determined residual stresses,

[2)] - a difference between the averaged residual stress and MFDM residual stress,

[3)] - relative difference calculated with respect to the averaged residual stress value.

6. Conclusions

The main conclusions drawn regarding the application of the MFDM discretization to the considered mechanical model may be stated as follows: the mixed global/local formulation of the MFDM has been successfully applied to solve an engineering problem and compute novel and interesting numerical solutions; the successful application of the MFDM requires thorough testing regarding the correct "star" size, weighting function and Taylor series truncation term for both global and local part of the formulation as well as the integration rule applied; in the considered problem the smallest reasonable (4 node in 2D) star size, the lowest order interpolating weighting function (factor p determined according to [15] for the first derivative) and the Taylor series truncated after the first derivative yielded consistently the best results; the Gauss integration between nodes of relatively low order (i.e. 2×2) is quite sufficient, though the quality of final results may suffer when the stress concentration happens to occur in the zones of skewed integration elements (i.e. in the corners of railhead); the boundary conditions affect the final solution very significantly, especially in the zones of low stress intensity, introducing the oscillations, which tend to propagate from the boundary towards the interior of the considered domain; of all tested, the integral fulfilment of the boundary conditions proved to be the one introducing the lowest errors to the interior of the domain.

Regarding the mechanical problem considered, i.e. one characterized by the localized very high concentrations of stresses and very high stress gradients in the adjacent zones, one may note that: the residual stress distributions computed on meshes of different densities seem to be very stable in term of location of tensile and compressive zones in the railhead, whereas the peak values of residual stresses tend to stabilize beginning with mesh #3, σ_{yy} seems to be the one notable exception here; therefore mesh #3 may be chosen as the basic mesh for the future calculations as the mesh offering the best compromise available between the computed solution quality and time spent on computation; two totally independent discrete methods (MFDM and HFEM) used to determine residual stresses yield results showing very good coincidence with respect to the stress component most important from the practical point of view (i.e. σ_{zz} residual stress) in qualitative terms, i.e. spatial distribution and shape of the tensile and compressive zones, in quantitative terms the extreme stress values are of comparable range (see Table 1, 2); other stress components show the same tendency with the exception of σ_{yy} residual stress; the erratic behaviour of the σ_{yy} stress component is certainly influenced by the fact, that this stress has the lowest values, and as such is most prone to the calculation errors; the computed results are reliable and obtained with reasonable engineering precision.

It is noteworthy, that the solution of the same mechanical problem using an independent (Zarka based [23]) mechanical model and h-adaptive FEM code has led to very similar numerical results in spite of significant modelling differences at

mechanical (incompressibility of plastic strains) as well as numerical (different numbers of nodal DOF's, differences in approximation and the application of boundary conditions), thus further validating the numerical approach presented here.

7. Further Research Proposed

It has been found out, that the boundary conditions and the integration quality present the most significant obstacles to further improvement in the quality of results. Therefore, improvements in these two areas are currently given the highest priority. Later on an attempt will be undertaken at improving the quality of results in the transition zones between the nodal meshes significantly differing in density. The currently obtained results in such cases are still not satisfactory [28]. After that the modern numerical techniques, such as a'posteriori error estimation and error analysis, based on results computed so far on meshes of various density, could be applied to adaptively refine these meshes, thus decreasing the size (number of nodes and variables) of problems to be solved, at the same time enhancing the quality of obtained solutions, by precisely controlling the errors committed during solution process.

References

1. Belytschko T., Lu Y.Y., Gu L.: Element-free Galerkin Methods, International Journal for Numerical Methods in Engineering, 37, 229-256, 1994.
2. Cecot W.: An Application of the Boundary Element Method to the Calculation of Residual Stresses Induced by Cyclic Loads, Ph.D. Thesis, SMI CUT, Cracow, 1989 (in polish).
3. Cecot W., Orkisz J.: Boundary Element Analysis of Actual Residual Stresses in Elastic- Plastic Bodies under Cyclic Loading, Int.J.Engng Anal. with Boundary Elements, 9/4, 289-292, 1992.
4. Cecot W., Orkisz J., Szczygiel M.: Boundary Element Analysis of Residual Stresses and Strains in a Railroad Rail, Proc. XI Conf. CMSM, Kielce-Cedzyna, 147-152, 1993.
5. Collatz L.: Numerische Behandlung von Differential Gleichungen, Springer, Berlin, 1955.
6. Dekker G.: Semi-discretization methods for partial differential equations on non-rectangular grids, International Journal of Numerical Methods in Engineering, 15, 405-419, 1980.
7. Forsythe G.E., Wasow W.R.: Finite Difference Methods for Partial Differential Equations, Wiley, New York, 1960.
8. Groom J.J.: Determination of Residual Stresses in Rails, Batelle Columbus Laboratories, Rpt. no. DOT/FRA/ORD-83-05, Columbus, 1983.
9. Holowinski M., Orkisz J.: Hybrid Finite Element Method for Estimation of Actual Residual Stresses. In: O.Orringer et al., editors, Residual Stress in Rails, II, 125-149, Kluwer Acad.Publ., 1992.
10. Jensen P.S.: Finite Difference techniques for variable grids, Computers and Structures, 2, 17-29, 1972.
11. Krok J., Orkisz J.: A unified approach to the FE and Generalized Variational FD method in nonlinear mechanics, concept and numerical approach, In: Discretization Method in Structural Mechanics, IUTAM/IACM Symposium, Vienna 1989, 353-362, Springer- Verlag, Berlin, 1990.
12. Krok J., Orkisz J.: On Adaptive Meshless FDM/FEM Approach in Field Problem, XIV Conf. PCMM, Rzeszów, 175-176, 1999.

13. Kwok S.K.: An improved curvilinear Finite Difference (CFD) method for arbitrary mesh systems, Computers and Structures, 18, 719-731, 1984.
14. Liszka T.: An interpolation method for an irregular net of nodes, International Journal of Numerical Methods in Engineering, 20, 1599-1612, 1984.
15. Liszka T., Orkisz J.: Finite Difference Method of Arbitrary Irregular Meshes in Non- Linear Problems of Applied Mechanics, 4th Int. Conf. on Structural Mechanics in Reactor Technology, San Francisco, California, 1977.
16. Liszka T., Orkisz J.: The finite difference at arbitrary irregular grids and it's applications in applied mechanics, Computers and Structures, 11, 109-121, 1980.
17. Liszka T., Orkisz J.: The Finite Difference Method for arbitrary irregular meshes - a variational approach to applied mechanics problems, Proc 2nd International Congress on Numerical Methods in Engineering, Paris, 277-288, 1980.
18. Liu W., Chen Y., Jun S., Chen J.S., Belytschko T., Pan C., Uras R.A., Chang C.T.: Overview and applications of the Reproducing Kernel Particle Methods, Archives of Computational methods in Engineering: State of the art reviews, 3, 3-80, 1996.
19. MacNeal R.H.: An asymmetrical Finite Difference network, Questions of Applied Mathematics, 11, 295-310, 1953.
20. Martin J.B.: Plasticity - fundamentals and general results, The MIT Press Publ., 1975.
21. Mullord P.: A general mesh finite difference method using combined nodal and elemental interpolation, Applied Mathematical Modelling, 3, 433-440, 1979.
22. Nayroles B., Touzot G., Villon P.: Generalizing the Finite Difference Method: diffuse approximation and diffuse elements, Computational Mechanics, 10, 307-318, 1992.
23. Oñate E., Idelsohn S.R.: A mesh-free finite point method for advective-diffusive transport and fluid flow problems, Computational Mechanics, 21, 283-292, 1998.
24. Orkisz J.: Finite Difference Method, In: M.Kleiber, editor, Handbook of Computational Solid Mechanics, 336-432, Springer Verlag, Berlin, 1998.
25. Orkisz J., Cecot W.: Prediction of actual residual stresses resulting from cyclic loading in kinematic hardening material, Proc. Int. Conf. COMPLAS V, Barcelona, 1879-1891, 1997.
26. Orkisz J., Harris A.: Analysis of Residual Stresses at Shakedown, A Hybrid Approach, Theoretical and Applied Fracture Mechanics, 9, pp. 109-121, 1988.
27. Orkisz J., Holowinski M.: Prediction of Residual Stresses in Rail: Practical Benefits from Theoretical Approach. In: J.J.Kalker et al., editors, Rail Quality and Maintenance for Modern Railway Operation, 273-285, Kluwer Acad.Publ., 1993.
28. Pazdanowski M.: Recent developments in estimation of residual stresses in railroad car wheels made of material exhibiting kinematic hardening, Proc. XV Conf. CMM, Gliwice/Wisla, 2003.
29. Peronne N., Kao R.: A general Finite Difference Method for arbitrary meshes, Computers and Structures, 5, 45-58, 1975.
30. Samarski A.A.: Theory of Difference Schemas, Nauka, Moscow, 1977. (in russian).
31. Skrzypek J.: Theory of Plasticity and Creep; Theoretical Introduction, Examples, Problems, Cracow University of Technology Press, Cracow, 1980. (in polish).
32. Sulsky D., Schreyer H.L.: The particle in cell method as a natural impact algorithm, Sandia National Labs, Contract No. AC-1801, 1993.
33. Wyatt M.J., Daves G., Snell C.: A new diference based Finite Element Method, Proceedings of Institute of Civil Engineering, 59, 395-409, 1975.
34. Zerbst U., Lunden R., Edel K.-O., Smith R.A.: Introduction to the damage tolerance behaviour of railway rails – a review, Engineering Fracture Mechanics, 76, pp. 2563-2601, 2009.
35. Zhang X., Liu X-H., Song K-Z., Lu M-W.: Least squares collocation meshless method, International Journal for Numerical Methods in Engineering, 51, 1089-1100, 2001.
36. Życzkowski M.: Combined Loadings in the Theory of Plasticity, Polish Scientific Publishers, 1981.